Journal of the American Statistical Association

ISSN: 0162-1459 (Print) 1537-274X (Online) Journal homepage: https://www.tandfonline.com/loi/uasa20

Calibrating Functional Parameters in the Ion Channel Models of Cardiac Cells

Matthew Plumlee, V. Roshan Joseph & Hui Yang

To cite this article: Matthew Plumlee, V. Roshan Joseph & Hui Yang (2016) Calibrating Functional Parameters in the Ion Channel Models of Cardiac Cells, Journal of the American Statistical Association, 111:514, 500-509, DOI: 10.1080/01621459.2015.1119695

To link to this article: https://doi.org/10.1080/01621459.2015.1119695

JOURNAL OF THE AMERICAN STATISTICAL ASSOCIATION
2016, VOL. 111, NO. 514, 500–509, Applications and Case Studies
http://dx.doi.org/10.1080/01621459.2015.1119695

Taylor & Francis
Taylor & Francis Group

Calibrating Functional Parameters in the Ion Channel Models of Cardiac Cells

Matthew Plumlee, V. Roshan Joseph, and Hui Yang

ABSTRACT
Computational modeling is a popular tool to understand a diverse set of complex systems. The output from a computational model depends on a set of parameters that are unknown to the designer, but a modeler can estimate them by collecting physical data. In the described study of the ion channels of ventricular myocytes, the parameter of interest is a function as opposed to a scalar or a set of scalars. This article develops a new modeling strategy to nonparametrically study the functional parameter using Bayesian inference with Gaussian process prior distributions. A new sampling scheme is devised to address this unique problem.

ARTICLE HISTORY
Received June 2014
Revised October 2015

KEYWORDS
Calibration; Computer experiment; Functional response; High-dimensional parameters; Simulation experiment

1. Introduction

The practice of positing and verifying a computational model is commonly used to investigate hypotheses about complex objects. Often, these models are defined up to a set of unknown parameters that are estimated by aligning the model's response with the observations (Box and Hunter 1962; Kennedy and O'Hagan 2001; Ramsay et al. 2007; Higdon et al. 2008; Arendt, Apley, and Chen 2012; Pratola et al. 2013; Monteiro, Banerjee, and Ramachandran 2014; Joseph and Yan 2015). The knowledge of the parameters' estimated value not only provides a better predictive model but also furthers the modelers' understanding of the system. Parameters discussed in the works of Bayarri et al. (2007) and Higdon et al. (2008) include important physical constants such as melting temperatures and reaction rates.

The existing methods proved insufficient for the discussed study of the ion channels in cardiac cells. Typically, one first isolates some set of parameters in the conjectured model. The parameters for recently proposed models of the ion channels originated from empirically defined functions. Instead of acquiescing in this formulation, this article considers the parameter of interest to be a function. Data are collected from a physical experiment that holds the input to the functional parameter constant and captures the behavior of the response. We infer about the functional parameter via a posterior distribution that melds the observations with a functional prior distribution.

This work also presents an alternative to the existing empirical methods used to study ion channels. The data used for our study were collected and first analyzed by Ednie et al. (2013). Following standard approaches, Ednie et al. first used least squares to fit exponential models to recordings of membrane current over time. Then the fitted exponential constant, termed the time constant, was used to make inferences on the system. This method is popular in the study of ion channels and these techniques have been employed to calibrate and justify computational models (Clancy and Rudy 1999; Stocker and Bennett 2006; Montpetit et al. 2009). This can be called a projection method, which is not necessarily an incorrect approach provided the projection preserves the features present in the data (Higdon et al. 2008). However, an examination of the longitudinal responses shows they are dissimilar from exponential shapes. This existing projection method may thus have a tempered capability to draw meaningful conclusions. In this work, inferential tools are designed to meet the exigent demand for new methods.

This article will discuss background in Section 2 followed by statistically motivated modifications and observations in Section 3. Section 4 and Section 5 will precisely define the model with functional parameters and the algorithm used to sample from the posterior. Finally, Section 6 will detail discoveries made during this case study. Some of these results contradict portions of knowledge observed in the existing literature on cardiac cell ion channels.

2. Background

This work studies the electrical activity of myocytes (muscle fiber cells) located on a heart's ventricle walls. When activated, ion channels located on the boundary of the cell allow for the influx and efflux of ions through the channels generating electrical currents. The time course of this activity is referred to as action potential of the ventricular myocytes. A steady recurrence of the depolarization and repolarization of these myocytes aggregates to the rhythmic, steady behavior of the heart. Slight changes in channel kinetics can alter the action potential waveform, and potentially cardiac excitation and conduction. For additional background on the general conceptual basis for cardiac cell ion channels, see Hille (2001) (or Grant (2009) for a more condensed summary).

Hodgkin and Huxley (1952) formulated the first cell action potential model using a set of nonlinear and ordinary differen-

CONTACT Matthew Plumlee mplumlee@umich.edu Department of Industrial and Operations Engineering, University of Michigan, Ann Arbor, MI 48109.
Color versions of one or more of the figures in the article can be found online at www.tandfonline.com/r/JASA.

tial equations. This original model was not designed for cardiac cells. Subsequent models of cardiac cells were developed to simulate the action potential through the ion channels; see the review of Noble, Garny, and Noble (2012). These models of transmembrane ionic currents consider ion channel kinetics as well as ionic concentrations. Different species and regions of the heart yield vastly different electrophysiological behaviors. This article borrows a model of ion channels from research with similar conditions to this case study on mouse cardiac cells. The impactful article by Clancy and Rudy (1999) was used by Bondarenko et al. (2004) to mimic the action potential of ventricular myocytes in adult mice; thus, Clancy and Rudy's model is adopted.

The membrane potential, denoted by the function of time $\mathrm{v}(\cdot)$, is the potential difference between the intracellular and extracellular sides of the cell. The current $\mathrm{i}(\cdot)$ is composed of several transmembrane currents grouped by the ion being transported, either sodium, potassium, or calcium. The model of Clancy and Rudy (1999) is based on the principle of the opening and closing of ion channels, known as gating. Research has shown that closed states can be further broken down into inactive and closed states. While in both states no current occurs, the inactive states are much less likely to move into an open state. It is possible for a channel to undergo movement from either an open or a closed state to an inactivated state.

The data consist of recorded current through only the sodium channels in a cell membrane. The current flowing through sodium channels can be represented by

$$\mathrm{i}(t) = G\mathrm{o}(t)(\mathrm{v}(t) - \mathrm{e}(t)),$$

where G is a conductance parameter that determines the dynamic ion permeation of the cell, $\mathrm{o}(t)$ is the proportion of open channels at time t, and $\mathrm{e}(t)$ is the channel reversal potential at time t. A key point here, which will be directly addressed soon, is that the *dynamics* of o depend on the membrane potential, v. The form of $\mathrm{e}(t)$ is given by $\mathrm{e}(t) = RT/F \cdot \log(\mathrm{Na}_0/\mathrm{Na}_\mathrm{i})$, where R, T, and F are physical constants and Na_0 and Na_i are the extracellular and intracellular sodium concentrations. The intracellular sodium concentrations will change with the flow of ions.

The data are observations from a voltage clamp experiment. The voltage-clamp method is a laboratory technique used to study currents passing through the cell membrane (Huxley 2002; Bear, Connors, and Paradiso 2007). In the voltage-clamp experiment, electrodes are placed in the intracellular and extracellular space. Starting at time zero, the transmembrane voltage is held at a predefined level and ionic currents flow through the membrane. Both electrodes are connected to an amplifier that measures the membrane voltage. At the same time, a signal generator can input an external voltage (a holding potential) to the cell. In the patch clamp experiment (Neher, Sakmann, and Steinbach 1978), the operator uses a glass micropipette with an open tip diameter of about one micrometer as an electrode. The micropipette is filled with a solution that is paired with the ionic composition of the bath solution. Careful selection of the intracellular and extracellular solutions in the patch clamp experiment allows for isolation of the sodium ion channels. A chloride silver wire is placed in the bath solution that conducts electric currents to amplifier. The data come from whole-cell recording that marks the currents through all ion channels over the entire membrane. More details on the collection of the data can be seen in Ednie et al. (2013).

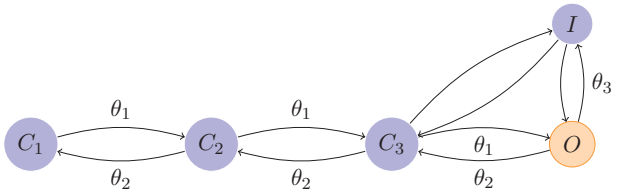

Figure 1. Diagram of the Markov model for the sodium channel. The states C_1, C_2, and C_3 represent closed states, O represents the open state, and I represents the inactive state. The labels θ represent dynamic transition rates that depend on membrane potential v. An unlabeled transition implies the transition rate is comparatively small according to Clancy and Rudy (1999).

3. Modified Computational Model

The chosen model for $\mathrm{o}(t)$ is described in detail in Appendix A and contains three unknown parameters $\{\theta_i\}_{i=1}^3$. This model was closely borrowed from Clancy and Rudy (1999). Consider a single ion channel that behaves according to the continuous time Markov model in Figure 1. During voltage clamp experiments, the channel starts in the closed state C_1, where no ions pass through the channel and thus no current flows. Similarly, when the channel is in the states C_2 and C_3, no current can flow. An ion channel will allow ions to pass when in the state O. The channel state labeled I is an inactivated closed state and the transition rates away from this state are small during these voltage clamp experiments. There are several simplifications from the model in Clancy and Rudy (1999). This model does not include an inactivation state that occurs only on extremely long lengthscales and is unlikely to be present in these observations. Our model groups parameters with similar values in Clancy and Rudy (1999). The model is approximated by assuming all transition rates not listed on the model diagram are zero over the short course of the voltage clamp experiment. Given the parameters of the original model of Clancy and Rudy (1999), these modifications represent setting small values to zero. This means no reactivation once a channel is deactivated until the voltage clamp is released, when the channel is reset to state C_1. If N channels independently behave according to this stochastic model, then as $N \to \infty$ the proportion of cells in each state converges to the proposed model (also known as the fluid limit (Kurtz 1971)).

For this analysis, the model is respecified by leveraging the specific conditions of the voltage clamp experiment. An important subtlety in this model is that the parameters of the channel gating dynamics, $\{\theta_i\}_{i=1}^3$, depend on the membrane potential. From time zero onwards, the value of $\mathrm{v}(t)$ is held at a constant. Thus, the parameters of the channel gating dynamics, $\{\theta_i\}_{i=1}^3$, are constant during voltage clamp experiments.

This idea simplifies the analysis greatly. Let the term $\boldsymbol{\theta}(v)$ mean $\{\theta_i\}_{i=1}^3$ for a fixed voltage v. Plugging this relation into the model, the response from voltage clamp experiments with held membrane potential v can be modeled by

$$\mathrm{i}(t) = G\mathrm{o}(t; \boldsymbol{\theta}(v))(v - \mathrm{e}(t)),$$

where $o(t; \boldsymbol{\theta}(v))$ is the proportion of open channels in open states at time t when the transition rates are $\boldsymbol{\theta}(v)$.

The slow dynamics of intracellular sodium accumulation imply that only minor intracellular sodium change occurs during the voltage clamp protocol, possibly due to the natural regularization (Bueno-Orovio et al. 2014). Therefore, an approximate model is

$$i^*(t, v; \boldsymbol{\theta}(\cdot)) = Go(t; \boldsymbol{\theta}(v))(v - E), \tag{1}$$

where E is a constant value across all clamp experiments. This new function is denoted as i^* to emphasize the modifications. The motivation for this change is practical as well as physical. The inference on the parameters of interest is conducted using a Gibbs sampler on the posterior distribution of the parameters. The current i^* as a function of t depends only on o, which is the solution of a set of ordinary linear differential equations; see Appendix A. Since this solution can be computed quickly, the inference is computationally feasible. We must also acknowledge the existence of inexactness when using this model. The discrepancy function modeling described in Section 4.3 accounts for these discrepancies.

4. Statistical Modeling

The voltage clamp experiment yields observations $y(t_k, v_j)$ for time points $t_1, \ldots, t_N$ and clamped membrane potentials $v_1, \ldots, v_M$. In the interest of compact notation, we denote $\{y(t_k, v_j)\}_{k=1,\ldots,N;\, j=1,\ldots,M}$ as simply the term "data." The major statistical novelty of this work is the ability to infer on a functional parameter $\boldsymbol{\theta}(\cdot)$. This section establishes a nonparametric statistical model for the functional parameter $\boldsymbol{\theta}(\cdot)$. The statistical model accounts for unknown parameters as well as potential model inadequacy.

4.1. Roadmap of Bayesian Statistical Modeling

We will conjecture about $\boldsymbol{\theta}$ by taking on the Bayesian viewpoint (Gelman et al. 2014). This perspective enables us to leverage the rich literature history on ion channels and account for the limited data from physical cells. Let π generally denote a probability density of a random variable and $\pi(a|b)$ be the probability density of a conditional on b. To conduct inference, a prior distribution is placed on $\boldsymbol{\theta}$ termed $\pi(\boldsymbol{\theta}(\cdot))$. This is done in Section 4.2. The goal is to find the posterior distribution of $\boldsymbol{\theta}(\cdot)$ based on the observations, $\pi(\boldsymbol{\theta}(\cdot)|\text{data})$. Using Bayes rule,

$$\pi(\boldsymbol{\theta}(\cdot)|\text{data}) \propto \pi(\text{data}|\boldsymbol{\theta}(\cdot))\pi(\boldsymbol{\theta}(\cdot)),$$

where $\propto$ indicates equality up to a constant multiplier and $\pi(\text{data}|\boldsymbol{\theta}(\cdot))$ is the distribution of the data given $\boldsymbol{\theta}(\cdot)$. This is often termed the *statistical model* of the data and is outlined in Section 4.3. Finally, it is often the case that the statistical model can be specified up to some *auxiliary parameters*, which are labeled $\boldsymbol{\psi}$ and are assumed to have independent prior distributions from $\boldsymbol{\theta}(\cdot)$. The goal is then to find the joint distribution of $\boldsymbol{\theta}(\cdot)$ and $\boldsymbol{\psi}$,

$$\pi(\boldsymbol{\theta}(\cdot), \boldsymbol{\psi}|\text{data}) \propto \pi(\text{data}|\boldsymbol{\theta}(\cdot), \boldsymbol{\psi})\pi(\boldsymbol{\theta}(\cdot))\pi(\boldsymbol{\psi}).$$

The prior distribution $\pi(\boldsymbol{\psi})$ is discussed in Section 4.4. This gives us the functional form of the posterior distribution. The method for drawing samples from it is detailed in Section 5.

4.2. Prior Distribution on the Functional Parameters

Previous calibration studies in the literature have focused on inferring on scalars; see references in this article's introduction. The relationship between $\boldsymbol{\theta}$ and the membrane potential is a functional dependence as we can observe a response for any clamped membrane potential. Clancy and Rudy (1999) assumed that $\boldsymbol{\theta}$ follows empirical formulas, but this was found to be inferior to the proposed formulation. Thus, the modeling of parameters must depart here from previous statistical literature on calibration.

The Bayesian paradigm requires us to place a prior distribution on this function. We suggest a Gaussian process prior distribution. The Gaussian process is a distribution on continuous functions where any function evaluation has a Normal distribution, a collection of function evaluations has a multivariate Normal distribution, and thus conditional distributions of evaluations based on other evaluations are also Normal. The use of a Gaussian process model is inspired by the computer experiments literature such as Sacks et al. (1989) and Currin et al. (1991). This Gaussian process prior distribution is

$$\log\theta_i(\cdot) \overset{\text{indep.}}{\sim} \text{GP}(\mu_i(\cdot), \sigma_i^2 r(\cdot, \cdot)),$$

where μ_i is the mean function, σ_i^2 is a positive scalar, r is the correlation function, and indep. implies that the prior distribution of θ_i is independent of θ_k if $k \neq i$. In this case, $\log\theta_i(v)$ follows a Normal distribution with mean $\mu_i(v)$ and the covariance between $\log\theta_i(v)$ and $\log\theta_i(v')$ is $\sigma_i^2 r(v, v')$. The log transform is used because the parameters ought to be positive but the Gaussian distribution has positive measure over the negative reals. In the case study, an exponential correlation function is used for r with a lengthscale parameter of 10 mV, that is,

$$r(v, v') = \exp(-|v - v'|/10).$$

The lengthscale parameter is determined based on the anticipated change in parameter as voltage is changed. The mean scalar function $\mu_i(\cdot)$ is taken as a linear model with parameters $\boldsymbol{\beta}_i = (\beta_{i1}, \beta_{i2})^\mathsf{T}$, a column vector, that is, $\mu_i(v) = (1, v)\boldsymbol{\beta}_i = \beta_{i1} + \beta_{i2}v$.

4.3. Statistical Model

Owing to the ubiquitous Kennedy and O'Hagan (2001) Bayesian formulation of the calibration problem, the difference between the observations y and i^* is composed of two elements. The first is the typical stochastic random error due to some source of noise. The second component is a *discrepancy function* termed b that represents possible differences between i^* and reality. This is a result of nature not aligning perfectly with the chosen model. Some potential sources of discrepancy are discussed in Section 3 but it is by no means an exhaustive list. For example, while conducting the experiment there was a small deviation in the clamped voltage due to controller dynamics (Ednie et al. 2013).

The discrepancy is not known exactly, but if the model is accurate the discrepancy will be small and the converse is true. The observed current for a given time point and clamped membrane potential is thus given by

$$y(t_k, v_j) = \mathrm{i}^*(t_\mathrm{k}, v_\mathrm{j}; \boldsymbol{\theta}(\cdot)) + b(t_\mathrm{k}, v_\mathrm{j}) + \varepsilon_{k,j}.$$

The prior distribution on the function b is represented by a Gaussian process with zero mean and a covariance structure defined over both time and voltage. This implies the prior distribution is such that b is a continuous function over both time and voltage. A small change in either the time or the clamped membrane potential should elicit a similarly small change in both i* and b and therefore the observation y, which agrees with intuition. The mean of prior distribution on b is zero and the covariance between $b(t, v)$ and $b(t', v')$ is $\sigma_b^2 r_b((t, v), (t', v'))$, where σ_b^2 is a positive parameter and r_b is a correlation function defined on $\mathbb{R}^2 \times \mathbb{R}^2$. The perturbations represented by $\varepsilon_{k,j}$ are generated by small environmental influences that will differ upon each subsequent measurement. Thus, each $\varepsilon_{k,j}$ has a prior distribution of independent Normal distributions with mean zero and variance σ_ε^2, where σ_ε^2 is a positive parameter.

4.4. Prior Distribution for the Auxiliary Parameters

Some parameters can be fixed because their values are well studied and/or determined by physical constants, such as G and E. For some parameters, there is no a priori knowledge of their values, but their values can be gleaned from the data. Denote this group of parameters $\boldsymbol{\psi}$. As mentioned earlier in this section, a prior distribution can be placed on $\boldsymbol{\psi}$ thus enabling inference. In this model, prior distributions are placed on the parameters $\boldsymbol{\beta}_1, \boldsymbol{\beta}_2, \boldsymbol{\beta}_3, \sigma_1^2, \sigma_2^2, \sigma_3^2, \sigma_b^2$, and σ_ε^2. The chosen prior distribution with motivation are given in Appendix B.

5. Analysis

Having established a modeling framework, computational methods for conducting inference are needed. The conclusions will be reached by drawing samples from the posterior distribution of the parameters of interest. Unfortunately, the parameter space is infinite due to $\boldsymbol{\theta}(\cdot)$ being a functional parameter. Thus, developments are needed. This section will provide those developments in the form of a Gibbs sampler, see Gelman et al. (2014), that takes advantage of the structure of the model and data.

Consider the posterior distribution of $\theta_i(v)$, where v is any membrane potential not in $\{v_1, \ldots, v_M\}$. For notational simplicity, let $\boldsymbol{\Theta}$ represent the set $\{\boldsymbol{\theta}(v_j)\}_{j=1}^M$. Since the statistical model for data only depends on $\boldsymbol{\Theta}$ and $\boldsymbol{\psi}$,

$$\pi(\theta_i(v), \boldsymbol{\Theta}, \boldsymbol{\psi}|\text{data}) \propto \pi(\theta_i(v)|\boldsymbol{\Theta}, \boldsymbol{\psi}) \cdot \pi(\boldsymbol{\Theta}, \boldsymbol{\psi}|\text{data}).$$

This implies sampling from the posterior distribution of $\theta_i(v)$ for any v can be done by drawing $\boldsymbol{\Theta}$ and $\boldsymbol{\psi}$ from their posterior distribution and then drawing from $\pi(\theta_i(v)|\boldsymbol{\Theta}, \boldsymbol{\psi})$.

We first address generating draws from $\pi(\theta_i(v)|\boldsymbol{\Theta}, \boldsymbol{\psi})$. Because independent Gaussian process prior distributions are used, $\theta_i(v)$ given $\{\theta_i(v_j)\}_{j=1}^M$ is independent of $\{\theta_k(v_j)\}_{j=1}^M$ if $k \neq i$. Let $\tilde{\boldsymbol{\theta}}_i = \left(\log\theta_i(v_1), \ldots, \log\theta_i(v_M)\right)^\mathsf{T}$, $\tilde{\boldsymbol{\mu}}_i = (\mu_i(v_1), \ldots, \mu_i(v_M))^\mathsf{T}$, $\boldsymbol{r}(v) = (r(v, v_1), \ldots, r(v, v_M))^\mathsf{T}$, and $\boldsymbol{R}$ be the correlation matrix where the jkth element is $r(v_j, v_k)$. Then $\pi(\theta_i(v)|\boldsymbol{\Theta}, \boldsymbol{\psi})$ is a log-Normal distribution with mean parameter

$$\mu(v) + \boldsymbol{r}(v)^\mathsf{T}\boldsymbol{R}^{-1}\left(\tilde{\boldsymbol{\theta}}_i - \tilde{\boldsymbol{\mu}}_i\right)$$

and variance parameter

$$\sigma_i^2\left(r(v, v) - \boldsymbol{r}(v)^\mathsf{T}\boldsymbol{R}^{-1}\boldsymbol{r}(v)\right).$$

To sample from

$$\pi(\boldsymbol{\Theta}, \boldsymbol{\psi}|\text{data}),$$

this article will employ a specialized Gibbs sampler. These are used to sample from multivariate distributions by sampling from one value in the vector conditioned on all other values. This sampler will draw from $\pi(\boldsymbol{\Theta}|\text{data}, \boldsymbol{\psi})$ and $\pi(\boldsymbol{\psi}|\text{data}, \boldsymbol{\Theta})$ repeatedly, plugging in the most recent samples when conditioning. As this is repeated, the samples will approach $\pi(\boldsymbol{\Theta}, \boldsymbol{\psi}|\text{data})$. After initialization, use the following sampling protocol to get the nth sample after the $n-1$th sample:

Cyclic sampler Given initial values of $\{\boldsymbol{\theta}(v_k)^{(n-1)}\}_{k=1}^M$. For $j = 1, \ldots, N$, draw $\boldsymbol{\theta}(v_j)^{(n)}$ given the data, $\boldsymbol{\psi}$, $\{\boldsymbol{\theta}(v_k)^{(n)}\}_{k<j}$, and $\{\boldsymbol{\theta}(v_k)^{(n-1)}\}_{k>j}$ via a Metropolis Hastings step or several Metropolis Hastings steps. The acceptance probability of a step is given in Equation (A.2).

In general, this should be iterated sufficiently to reach convergence to the distribution of $\boldsymbol{\Theta}$ conditioned on $\boldsymbol{\psi}$ and the data. This algorithm cycles through the sampling of the parameter $\boldsymbol{\theta}$ at v_j for all j. The benefit of using the above sampler is instead of attempting to estimate a single $3M$ sized parameter $\{\boldsymbol{\theta}(v_j)\}_{j=1}^M$ we must only sample three-dimensional parameters $\boldsymbol{\theta}(v_j)$. The efficiency gain comes from the fact that the posterior distribution of $\boldsymbol{\theta}(v_j)$ depends heavily on the likelihood of the observations $\{y(t_k, v_j)\}_{k=1,\ldots,N}$, which has strong dependence on $\boldsymbol{\theta}(v_j)$ through i* and only weak dependence on $\{\boldsymbol{\theta}(v_k)\}_{k\neq j}$ through the discrepancy term b and the prior distribution on the functional parameters.

This cyclic sampler can be used in concert with a typical Gibbs sampler. The exact algorithm that was used in the case study is outlined below. At any stage in the sampler, the next parameter values are drawn as follows:

1. Starting at the last sample of $\{\boldsymbol{\theta}(v_k)\}_{j=1}^M$, use the cyclic sampler to get samples of $\{\boldsymbol{\theta}(v_k)\}_{j=1}^M$ given the data and the latest sample of all other parameters.
2. For each $i = 1, \ldots, 3$, use the distribution defined at the end of Appendix C to draw σ_i^2 directly from the conditional posterior distribution of σ_i^2 given the data and the latest sample of all other parameters. Then use the distribution defined at the end of Appendix C to draw $\boldsymbol{\beta}_i$ directly from the conditional posterior distribution of $\boldsymbol{\beta}_i$ given the data and the latest sample of all other parameters. Repeat this step several times to get samples of σ_i^2 and $\boldsymbol{\beta}_i$.
3. Draw σ_ε^2 and σ_b^2 using Metropolis Hastings steps on conditional posterior distribution of σ_ε^2 and σ_b^2 given the data and the latest sample of all other parameters.

In the following section, the analysis drew every fifth sample (for small storage) to collect 250 samples and established an

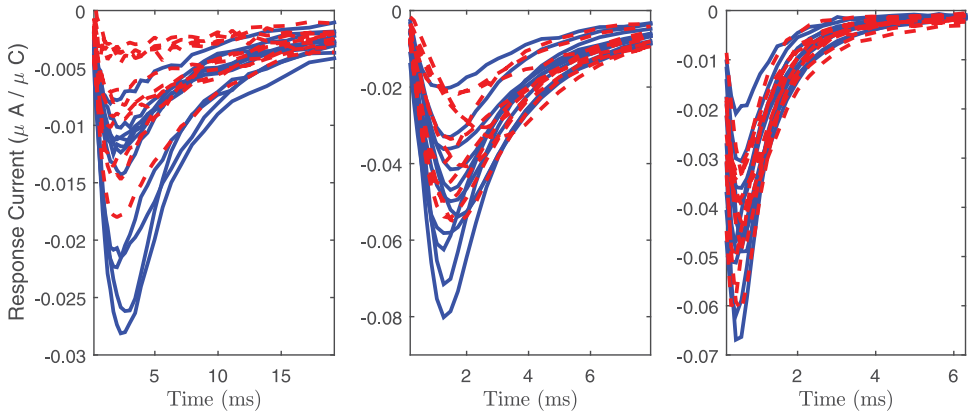

Figure 2. Collected responses for wild-type (solid) and ST3Gal4-deficient (dashed) during three separate clamped voltage experiments, −55 mV (left), −45 mV (middle), −15 mV (right).

average effective sample size of 175 for all parameters $\boldsymbol{\Theta}$ (Kass et al. 1998).

The posterior distribution of $y(t, \upsilon)$, used in the next section, is detailed in Appendix C.

6. Case Study: The Effect of Aberrant Sialylation

6.1. Experimental Data

This section leverages the statistical developments to investigate two groups of physical cells denoted "wild-type" and "ST3Gal4-deficient." The ST3Gal4-deficient subjects are lacking the enzyme β-galactoside α-2,3-sialyltransferase 4 (ST3Gal4), which is 1 of 20 sialyltransferase enzymes that increase sialic acids in galactose residues (Montpetit et al. 2009; Ednie and Bennett 2012; Du et al. 2014). The ST3Gal4-deficient strain has been used to investigate the general problem of aberrant glycosylation in cardiovascular function. The wild-type subjects were generated with proper production of the ST3Gal4 enzyme.

The data consist of the results after experiments were conducted on 11 wild-type and 11 ST3Gal4-deficient cells selected from Ednie et al. (2013). These were deemed successful experiments based on visual inspection. Each cell was studied via clamped voltage excitation with clamped membrane potentials ranging from −65 mV to 0 mV in 5 mV increments. The response at −40 mV was excluded for a posterior check seen in Figure 3. The data collection was documented and first analyzed in Ednie et al. (2013). The response current was saved at nonuniformly spaced samples in time to account for the greater deal of variability in the run-up. Following the analysis of Ednie et al. (2013), the response y was normalized to account for cell size differences by dividing a separately measured capacitance value. This allows us to set the G value as outlined in Appendix B. It also implies that the y values and i^* values will be reported in units of $\mu A/\mu C$. Efforts were made to ensure that the data are properly aligned but we acknowledge this is inexact.

Figure 2 shows the responses for three different membrane potentials. There is a significant subject to subject difference. To account for this observation, Bayesian method is used to sample from the posterior distributions corresponding to individual cell data.

The ST3Gal4-deficient cells appear to behave separately from the wild-type cells especially at low membrane potentials. The goal here is to reach some conclusions about the possible mechanism behind this effect. The prevailing paradigm for this type of study involves two steps. First, one conjectures a model for differences between the cells. Second, through a series of empirical comparisons one shows that the conjectured model is a superior representation of the modified cells. For example, Clancy and Rudy (1999) studied the effect of a different mutation on action potential and give biophysical justifications for a new model for the ΔKPQ mutated cells. Parameters of their Markov model are fixed in both wild-type and mutated cells. This allows claims such as "mutant channels activate more quickly." The affirmations are based on the reported time constants described in the introduction. Here we make four observations that distinguish this analysis from the previous literature: (i) the longitudinal

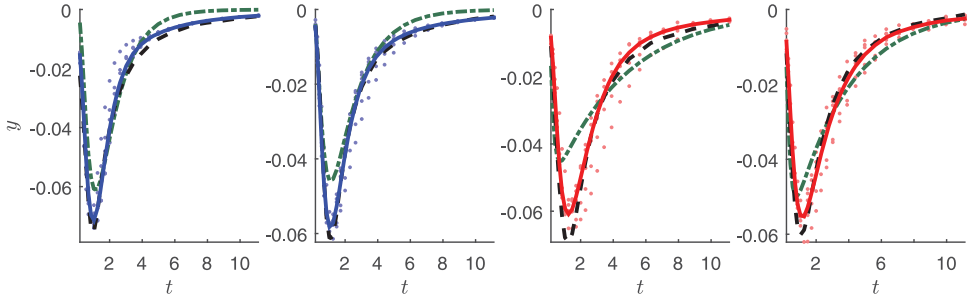

Figure 3. Observed response (dashed-line) and predicted responses using least squares calibration with the original parameters (dashed-dotted line) and the posterior distribution's mean (thick solid) with five draws from the posterior distribution represented by dots. The response corresponds to a clamped membrane potential of −40 mV for two wild-type cells (left) and two ST3Gal4-deficient cells (right).

responses can be modeled physiologically, (ii) the parameters of the computational model are uncertain, (iii) there is possibly a gap between this model and reality, and (iv) the specific behavior of a cell can radically differ between subjects. The Bayesian framework discussed incorporates all of these observations.

6.2. Results and Conclusions

The success of the analysis hinges on the adequacy of the model described in Sections 3 and 4. As an initial model check, Figure 3 shows the posterior distribution of withheld data using the proposed approach. We predict the response to a clamped membrane potential of −40 mV using the observations from experimental results at −65 mV, −60mV ..., −45 mV, −35 mV, ..., 0 mV. The posterior distribution's mean is compared to a standard least squares calibration using the parameterized form of $\theta(\cdot)$ proposed by Clancy and Rudy (1999). The posterior distribution seems reasonable and there appears to be improvement for prediction over the more traditional least squares approach.

An important initial question is if the model of the response, i*, is sufficient to describe the observed behavior. If i* is extremely different from y, the resultant posterior distributions of parameters such as $\boldsymbol{\theta}(\cdot)$ will be of little significance (and likely indistinguishable from the prior distribution). This is measured by the discrepancy function, b. A small discrepancy implies the model fits the data well and a large discrepancy implies the opposite. Figure 4 shows posterior distributions of discrepancy function using data from two different cells, one of which is wild-type and the other of which is ST3Gal4-deficient. The discrepancy function appears small, and this figure is representative of all cells. This supports the idea that the described model may be sufficient for describing both wild-type and ST3Gal4-deficient cells. One additional observation is that the discrepancy function contains some high-frequency behavior. Future studies of ion channels may require more complex models if this behavior is of primary interest.

The values of θ_1, θ_2, and θ_3 represent the rates at which channels open, close, and inactivate, respectively. Figure 5 displays the posterior distribution of θ_1, θ_2, and θ_3 for a dense set of voltages in our study. Because the parameters are defined as functions, their posterior distributions can be visualized. The lower half of Figure 5 displays the *average posterior distribution,* which is constructed by drawing parameters for each cell and taking the sample average among the wild-type and ST3Gal4-deficient groups, denoting the average with an overbar. In general, the 90% credible interval for a single cells' posterior distributions is broader than the average posterior distributions. This variation reduction is a natural result achieved by averaging. In general, all parameters appear to be reasonably close to monotonic in the membrane potential. The strongest trend lies in the rate of opening, which increases as membrane potential is increased. Comparatively, the inactivation of cells is nearly constant across all voltages.

We can now move to the main goal of conjecturing about the differences between the two groups of cells in terms of the posited model. To do so, we compute samples of the ratio of the average for all wild-type cells divided by the average for ST3Gal4-deficient cells. The posterior distribution of this value is seen in Figure 6. If the posterior distribution is concentrated around a value bigger than 1, then ST3-deficient cells have a smaller value of θ_i. If the posterior distribution is concentrated around a value smaller than 1, then ST3-deficient cells have a larger value of θ_i. At low membrane potentials, it appears that the ST3-deficient cells have a slower transition rate to the open state. This effect appears to disappear at high membrane potentials. These results align with the conclusions published in Ednie et al. (2013). There is not similarly strong conclusions about the closing or inactivation transition rates based on this dataset. There appears to be some evidence for Ednie et al.'s (2013) claim that ST3Gal4-deficient cells "inactivated more slowly," though the evidence is not striking enough to completely affirm their conclusion. The fact that these conclusions are weaker than the ones produced by Ednie et al.'s data analysis is expected. This article accounts for many things, including model discrepancy and auxiliary parameter uncertainty, which are often ignored in time constant reporting.

7. Discussion and Future Work

This article has developed a method to infer on a functional parameter using Gaussian process prior distributions. We were able to investigate a model of the sodium ion channels in cardiac cells. The model specified for the sodium channel is designed for voltage clamp experiments. A possible future extension of this work is using other experimental studies to investigate parameters unable to be studied in this work, such as reactivation rates. Going forward, it will be interesting to investigate several other electrophysiological challenges. Action potential simulation requires the full functional form of $\theta(\cdot)$. It is not clear how to leverage the functional parameter's posterior distribution into

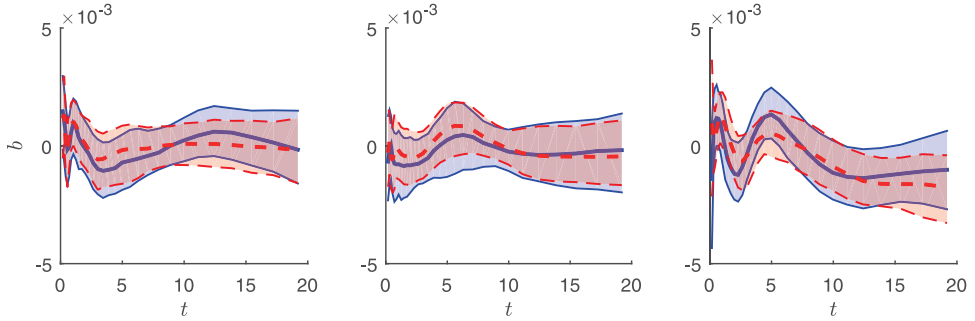

Figure 4. Pointwise medians and 90% credible intervals of the discrepancy function's posterior distribution for three different clamped membrane potentials, −55 mV (left), −45 mV (middle), and −15 mV (right). The solid lines are from a wild-type cell and the dashed lines are from a ST3Gal4-deficient cell.

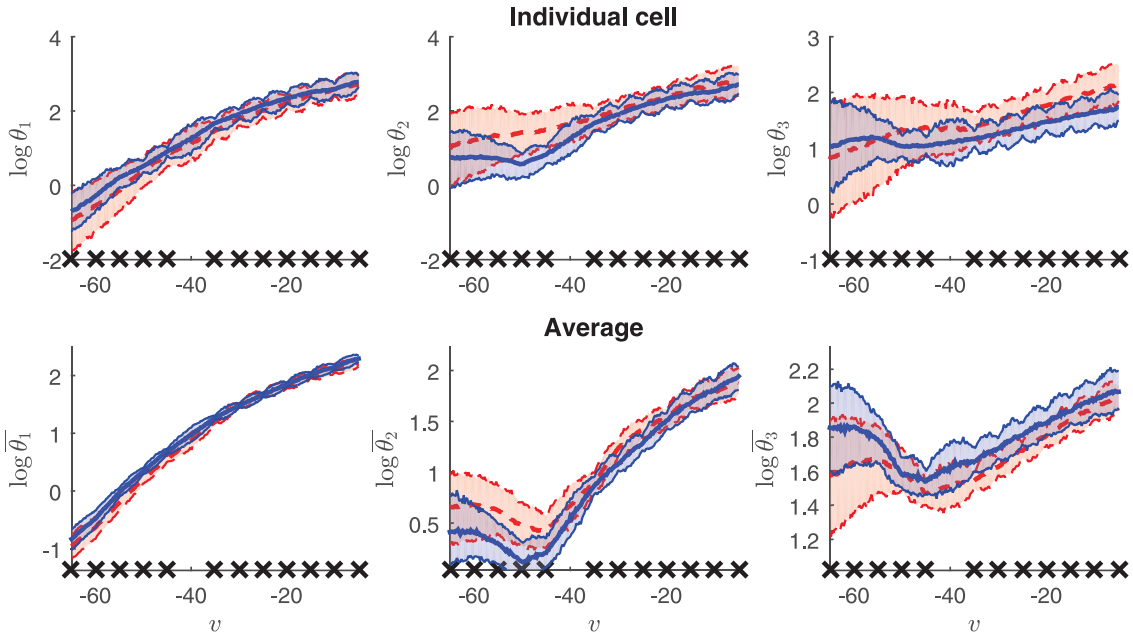

Figure 5. Pointwise medians and 5%, 95% quantiles of the posterior distribution of θ_1, θ_2, and θ_3. The top three plots correspond to two individual cell posterior distributions and the bottom plots display the information for average posterior distributions for each group. The solid lines are from wild-type cell(s) and the dashed lines are from ST3Gal4-deficient cell(s). The "x" tick marks represent observation points.

a computational model where the voltage can change. A simple implementation would use the posterior distribution's mean as a plug-in estimate. However, the uncertainty quantification will likely require some type of Monte Carlo method. Another complexity of single-cell experiments is that similar single-cell parameters might produce very different aggregate responses (e.g., Grashow, Brookings, and Marder 2009).

Using a Bayesian approach for electrophysiological systems can also account for the uncertainty in the estimated parameters. This could be critical for electrophysiological systems as there has been observations that multiple parameter combinations can produce similar outputs (see Achard and De Schutter (2006) for an example involving neurons). A wide posterior distribution indicates that creating a good parameter estimate would prove difficult based on the existing data. A narrower posterior distribution could assure a researcher that enough data was collected to conjecture about a parameter. Thus, this framework has the potential to make distinctions of significant differences in parameters easier for a researcher. As a comparison, Britton et al. (2013) used thousands of parameter combinations as a search mechanism to find appropriate model parameters. The Bayesian approach outlined here could serve as a substitute for that method. This analogy becomes more apparent if our sampling scheme was replaced with Approximate Bayesian Computation (Csilléry et al. 2010). In our work, the intersubject variability is addressed by isolating specific parameters for each cell in the study and sampling from their individual posterior distribution. The review of Sarkar, Christini, and Sobie (2012) indicates that variability expressed in the observations could be explained through parameters for electrophysiological cell models.

In addition to the future study of the electrical activity of cardiac cells, work is needed to infer on functional parameters in general cases. The conditional distributions require experiments where the environmental condition is held constant. In some systems, this is not possible. In these cases, more

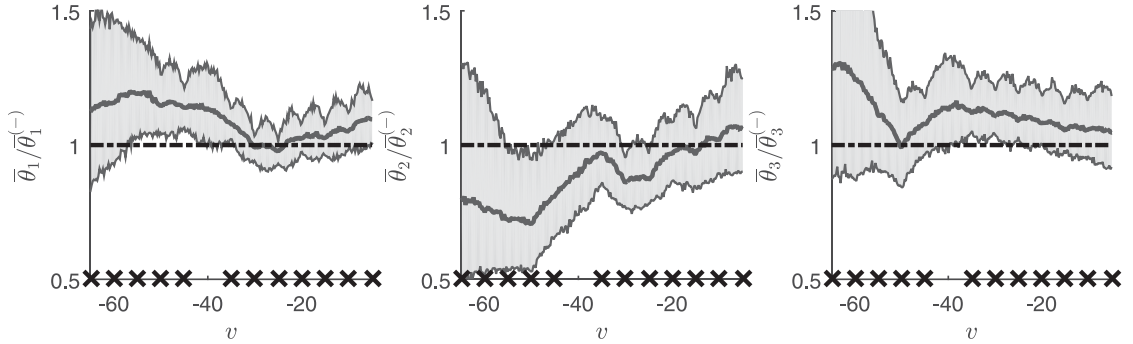

Figure 6. Pointwise medians and 5%, 95% quantiles of the ratio $\bar{\theta}_i(v)/\bar{\theta}_i^{(-)}(v)$, where $\bar{\theta}_i$ is the sample average of the parameters from wild-type cells and $\bar{\theta}_i^{(-)}$ is the sample average of the parameters ST3Gal4-deficient cells. The "x" tick marks represent observation points.

flexible tools are required. One idea for conducting inference is to use only function values corresponding to inputs on a fine mesh, thus making the problem finite dimensional. Research is needed to investigate sampling mechanisms that coordinate well with this framework (Cotter et al. 2013). Moreover, even in the case stated in the article, there is doubt as to whether the cyclic sampling approach to functional parameters is optimal. Since the prior distribution induces a correlation between function evaluations of the parameter, for example, $\theta_i(v_1)$ and $\theta_i(v_2)$, they will also have correlation in their posterior distribution. Therefore, approaches such as Hamiltonian Monte Carlo (Neal 2011) could outperform the method but they do come with the computational cost of gradient evaluation.

Appendix A: Differential Equation Model for o

The differential equation system for the ion channels is defined by

$$\frac{\mathrm{d}\boldsymbol{x}}{\mathrm{dt}} = \boldsymbol{A}(\boldsymbol{\theta})\boldsymbol{x},$$

where $\boldsymbol{x}$ is the vector of the proportion of ion channels in the C_3, O, C_2, and C_1 states and

$$\boldsymbol{A}(\boldsymbol{\theta}) = \begin{pmatrix} -\theta_1 - \theta_2 & \theta_2 & \theta_1 & 0 \\ \theta_1 & -\theta_2 - \theta_3 & 0 & 0 \\ \theta_2 & 0 & -\theta_1 - \theta_2 & \theta_1 \\ 0 & 0 & \theta_2 & -\theta_1 \end{pmatrix}.$$

Consider the voltage clamped experiments. Let $\boldsymbol{x}_0$ be the solution at time 0. For Section 6, $\boldsymbol{x}_0 = (0, 0, 0, 1)^{\mathsf{T}}$ since the cells were held at a very low voltage , -100 mV, prior to being held at the clamped voltage, thereby ensuring most ion channels are in the most closed position. Then,

$$o(t; \boldsymbol{\theta}) = x_2(t) = (0, 1, 0, 0)\exp(t\boldsymbol{A})\boldsymbol{x}_0.$$

Appendix B: Prior Distributions

For the model parameters θ_i, prior distributions are needed for σ_i and μ_i for each $i = 1, \ldots, 3$. We choose a prior on σ_i^2 of an inverse gamma with shape parameter 4 and rate parameter 1. This is a broad distribution with mean 1/3. For the prior on each $\boldsymbol{\beta}$ we choose multivariate Normal distribution with mean $(-1, 0)^{\mathsf{T}}$ and covariance matrix $\mathrm{diag}(1, (2/35)^2)$, which gives us a broad prior.

The priors on σ_ϵ and σ_b and correlation functions are:

- σ_ε^2 has an inverse gamma prior with shape parameter 100 and rate parameter 0.0001. This is a broad distribution with mean $0.0001/100 = (0.1/100)^2$ $(\mu A/\mu C)^2$.
- σ_b^2 has an inverse gamma prior with shape parameter 100 and rate parameter 0.000625. This is a broad distribution with mean $0.000625/100 = (0.25/100)^2$ $(\mu A/\mu C)^2$.
- r_b is the outer product of an exponential and Matérn covariance function with smoothness parameter 2.5,

$$r_b((t, v), (t', v')) = (1 + \sqrt{5}\Delta_t + 5\Delta_t^2/3) \exp(-\Delta_v - \sqrt{5}\Delta_t)),$$

where $\Delta_t = |\log(t) - \log(t')|$ and $\Delta_v = 5^{-1}|v - v'|$. The first difference function, Δ_t, was chosen to allow for more time-varying behavior in the run-up present in observations seen in Figure 2, possibly generated by the dynamics of the controller. It is also a correlation function corresponding to smoother outputs than the exponential (Handcock and Stein 1993).

Finally, G is set to a fixed value of 0.01 $\mu S/\mu C$ to prevent identifiability issues. This is consistent with the numbers used in Bondarenko et al. (2004). E is set to a fixed value of +20 mV based on the temperature during and ionic concentrations during the experiment.

Appendix C: Sampler and Prediction Details

For simplicity, denote $\boldsymbol{y}_j$ as the vectorization of $\{y(t_k, v_j)\}_{k=1,\ldots,N}$. From Bayes rule $\pi(\log\boldsymbol{\theta}(v_j)|\text{data}, \boldsymbol{\psi}, \{\log\boldsymbol{\theta}(v_k)\}_{k\neq j}) \propto \pi(\boldsymbol{y}_j|\{\boldsymbol{y}_k\}_{k\neq j}, \boldsymbol{\psi}, \{\log\boldsymbol{\theta}(v_k)\}_{k=1}^M)\pi(\log\boldsymbol{\theta}(v_j)|\{\log\boldsymbol{\theta}(v_k)\}_{k\neq j}, \boldsymbol{\psi}, \{\boldsymbol{y}_k\}_{k\neq j})$ and from our framework

$$\begin{aligned}&\pi(\log\boldsymbol{\theta}(v_j)|\{\log\boldsymbol{\theta}(v_k)\}_{k\neq j}, \boldsymbol{\psi}, \{\boldsymbol{y}_k\}_{k\neq j}) \\ &\quad = \pi(\log\boldsymbol{\theta}(v_j)|\{\log\boldsymbol{\theta}(v_k)\}_{k\neq j}, \boldsymbol{\psi}). \qquad \text{(A.1)}\end{aligned}$$

Using Equation (A.1),

$$\begin{aligned}&\pi(\log\boldsymbol{\theta}(v_j)|\{\log\boldsymbol{\theta}(v_k)\}_{k\neq j}, \boldsymbol{\psi}) \propto p_1(\log\boldsymbol{\theta}(v_j)|\{\log\boldsymbol{\theta}(v_k)\}_{k\neq j}, \boldsymbol{\psi}) \\ &:= \exp\left(-\frac{1}{2}\sum_{i=1}^{3}\sigma_i^{-2}\left(r(v, v) - \boldsymbol{r}_{-j}^{\mathsf{T}}\boldsymbol{R}_{-j}^{-1}\boldsymbol{r}_{-j}\right)^{-1}\left(\log\theta_i(v_j)\right.\right. \\ &\left.\left. - \mu_{i;j|-j}\right)^2\right),\end{aligned}$$

where

$$\mu_{i,j|-j} = \mu_i(v_j) + \boldsymbol{r}_{-j}^{\mathsf{T}}\boldsymbol{R}_{-j}^{-1}\left(\tilde{\boldsymbol{\theta}}_{i;-j} - \tilde{\boldsymbol{\mu}}_{i;-j}\right),$$

$\tilde{\boldsymbol{\mu}}_{i;-j}$, $\tilde{\boldsymbol{\theta}}_{i;-j}$, and $\boldsymbol{r}_{-j}$ are the same as their not subscripted counterparts in Section 5 with the jth element removed and $\boldsymbol{R}_{-j}$ is the prior correlation matrix of $\tilde{\boldsymbol{\theta}}_{i;-j}$.

We have left to find the conditional distribution of $\boldsymbol{y}_j$. Let $\boldsymbol{b}_j$ be the vectorization of $\{b(t_k, v_j)\}_{k=1,\ldots,N}$, $\boldsymbol{\varepsilon}_j$ be the vectorization of $\{\varepsilon_{k,j}\}_{k=1,\ldots,N}$, and let $\boldsymbol{i}(\boldsymbol{\theta})$ be the vectorization of $\{\mathrm{i}^*(t_k, v_j)\}_{k=1,\ldots,N}$ given $\boldsymbol{\theta}$. Then

$$\boldsymbol{y}_j = \boldsymbol{i}(\boldsymbol{\theta}(v_j)) + \boldsymbol{b}_j + \boldsymbol{\varepsilon}_j.$$

The value of $\boldsymbol{i}(\boldsymbol{\theta}(v_j))$ given $\boldsymbol{\theta}(v_j)$ and $\boldsymbol{\psi}$ is deterministic. The distribution $\boldsymbol{b}_j$ given $\{\boldsymbol{y}_k\}_{k\neq j}$ and $\{\boldsymbol{\theta}(v_k)\}_{k=1}^M$ is

$$\mathcal{N}\left(\hat{\boldsymbol{b}}_{b_j|y_{-j}}, \sigma_b^2\boldsymbol{R}_{b_j|y_{-j}}\right),$$

where

$$\hat{\boldsymbol{b}}_{b_j|y_{-j}} = \sigma_b^2\boldsymbol{R}_{b_j,b_{-j}}\left(\sigma_b^2\boldsymbol{R}_{b_{-j}} + \sigma_\epsilon^2\boldsymbol{I}\right)^{-1}\left(\boldsymbol{y}_{-j} - \boldsymbol{i}_{-j}\right),$$

$$\boldsymbol{y}_{-j} = \begin{pmatrix} \boldsymbol{y}_1 \\ \vdots \\ \boldsymbol{y}_{j-1} \\ \boldsymbol{y}_{j+1} \\ \vdots \\ \boldsymbol{y}_M \end{pmatrix}, \boldsymbol{i}_{-j} = \begin{pmatrix} \boldsymbol{i}(\boldsymbol{\theta}(\upsilon_1)) \\ \vdots \\ \boldsymbol{i}(\boldsymbol{\theta}(\upsilon_{j-1})) \\ \boldsymbol{i}(\boldsymbol{\theta}(\upsilon_{j+1})) \\ \vdots \\ \boldsymbol{i}(\boldsymbol{\theta}(\upsilon_M)) \end{pmatrix}$$

and

$$\boldsymbol{R}_{b_j|y_{-j}} = \boldsymbol{R}_{b_j} - \sigma_b^2 \boldsymbol{R}_{b_j,b_{-j}} \left(\sigma_b^2 \boldsymbol{R}_{b_{-j}} + \sigma_\epsilon^2 \boldsymbol{I}\right)^{-1} \boldsymbol{R}_{b_j,b_{-j}}^{\mathsf{T}}.$$

The matrix $\boldsymbol{I}$ is an identity matrix, $\boldsymbol{R}_{b_j}$ is the correlation matrix corresponding to $\boldsymbol{b}_j$, the matrix $\boldsymbol{R}_{b_{-j}}$ is the correlation matrix corresponding to

$$\boldsymbol{b}_{-j} = \begin{pmatrix} \boldsymbol{b}_1 \\ \vdots \\ \boldsymbol{b}_{j-1} \\ \boldsymbol{b}_{j+1} \\ \vdots \\ \boldsymbol{b}_M \end{pmatrix},$$

and the matrix $\boldsymbol{R}_{b_j,b_{-j}}$ is the cross-correlation matrix between the vectors. Combining the above, since the three terms $\boldsymbol{i}(\boldsymbol{\theta}(\upsilon_j))$,$\boldsymbol{b}_j$, and $\boldsymbol{\varepsilon}_j$ are independent and multivariate normal,

$$\begin{aligned} \pi(\boldsymbol{y}_j|\{\boldsymbol{y}_k\}_{k\neq j}, \boldsymbol{\psi}, \{\boldsymbol{\theta}(\upsilon_k)\}_{k=1}^M) &\propto p_2(\boldsymbol{\theta}(\upsilon_j)|\text{data}, \boldsymbol{\psi}, \{\boldsymbol{\theta}(\upsilon_k)\}_{k\neq j}) \\ &:= \exp\left(-\frac{1}{2}\left(\boldsymbol{y}_j - \boldsymbol{i}(\boldsymbol{\theta}(\upsilon_j)) - \hat{\boldsymbol{b}}_{b_j|y_{-j}}\right)^{\mathsf{T}} \left(\sigma_b^2 \boldsymbol{R}_{b_j|y_{-j}} + \sigma_\varepsilon^2 \boldsymbol{I}\right)^{-1} \right. \\ &\quad \left. \times \left(\boldsymbol{y}_j - \boldsymbol{i}(\boldsymbol{\theta}(\upsilon_j)) - \hat{\boldsymbol{b}}_{b_j|y_{-j}}\right)\right). \end{aligned}$$

Finally, the rejection rate used in our cyclic sampler described in Section 5 is

$$\begin{aligned} &\frac{\pi\left(\log\boldsymbol{\theta}(\upsilon_j)^{(n)}|\text{data}, \boldsymbol{\psi}, \{\log\boldsymbol{\theta}(\upsilon_k)^{(n)}\}_{k<j}, \{\log\boldsymbol{\theta}(\upsilon_k)^{(n-1)}\}_{k>j}\right)}{\pi\left(\log\boldsymbol{\theta}(\upsilon_j)^{(n-1)}|\text{data}, \boldsymbol{\psi}, \{\log\boldsymbol{\theta}(\upsilon_k)^{(n)}\}_{k<j}, \{\log\boldsymbol{\theta}(\upsilon_k)^{(n-1)}\}_{k>j}\right)} \\ &= \frac{p_1\left(\log\boldsymbol{\theta}(\upsilon_j)^{(n)}|\{\log\boldsymbol{\theta}(\upsilon_k)^{(n)}\}_{k<j}, \{\log\boldsymbol{\theta}(\upsilon_k)^{(n-1)}\}_{k>j}, \boldsymbol{\psi}\right)}{p_1\left(\log\boldsymbol{\theta}(\upsilon_j)^{(n-1)}|\{\log\boldsymbol{\theta}(\upsilon_k)^{(n)}\}_{k<j}, \{\log\boldsymbol{\theta}(\upsilon_k)^{(n-1)}\}_{k>j}, \boldsymbol{\psi}\right)} \\ &\times \frac{p_2\left(\boldsymbol{\theta}(\upsilon_j)^{(n)}|\text{data}, \boldsymbol{\psi}, \{\boldsymbol{\theta}(\upsilon_k)^{(n)}\}_{k<j}, \{\boldsymbol{\theta}(\upsilon_k)^{(n-1)}\}_{k>j}\right)}{p_2\left(\boldsymbol{\theta}(\upsilon_j)^{(n-1)}|\text{data}, \boldsymbol{\psi}, \{\boldsymbol{\theta}(\upsilon_k)^{(n)}\}_{k<j}, \{\boldsymbol{\theta}(\upsilon_k)^{(n-1)}\}_{k>j}\right)}. \end{aligned} \tag{A.2}$$

Let $\boldsymbol{y}^{\mathsf{T}} = [\boldsymbol{y}_1^{\mathsf{T}}, \ldots, \boldsymbol{y}_M^{\mathsf{T}}]$ and let $\boldsymbol{R}_b$ be correlation matrix corresponding to $\boldsymbol{b}^{\mathsf{T}} = [\boldsymbol{b}_1^{\mathsf{T}}, \ldots, \boldsymbol{b}_M^{\mathsf{T}}]$. The covariance matrix of $\boldsymbol{y}$ is

$$\boldsymbol{\Sigma}_y = \sigma_b^2 \boldsymbol{R}_b + \sigma_\varepsilon^2 \boldsymbol{I}.$$

Similar to the proceeding, $y(t,v)$ has posterior distribution

$$\mathcal{N}\left(\mathrm{i}^*(t, v; \boldsymbol{\theta}(\cdot)) + \hat{\mathrm{b}}_{b|y}(t, v), \sigma_{b|y}^2 + \sigma_\varepsilon^2\right), \tag{A.3}$$

where

$$\hat{b}_y(t, \upsilon) = \sigma_b^2 \boldsymbol{r}_b(t, \upsilon) \boldsymbol{\Sigma}_y^{-1} \left(\boldsymbol{y} - \boldsymbol{i}\right)$$

and

$$\sigma_{b|y}^2 = \sigma_b^2 - \sigma_b^4 \boldsymbol{r}_b(t, \upsilon) \boldsymbol{\Sigma}_y^{-1} \boldsymbol{r}_b^{\mathsf{T}}(t, \upsilon).$$

The matrix $\boldsymbol{R}_b$ is the correlation matrix corresponding to $\boldsymbol{b}$, and the vector $\boldsymbol{r}_b(t, \upsilon)$ is the correlation between $b(t, \upsilon)$ and $\boldsymbol{b}$.

Let the prior on σ_i^2 be an inverse gamma with shape parameter α_i and rate parameter γ_i. Given all other parameters, we can use standard analysis tools to find that the posterior distribution is an inverse gamma with shape parameter

$$\alpha_i + \frac{M}{2}$$

and rate parameter

$$\gamma_i + \frac{1}{2}\left(\tilde{\boldsymbol{\theta}}_i - \tilde{\boldsymbol{\mu}}_i\right)^{\mathsf{T}} \boldsymbol{R}^{-1} \left(\tilde{\boldsymbol{\theta}}_i - \tilde{\boldsymbol{\mu}}_i\right).$$

Let the prior on $\boldsymbol{\beta}_i$ be multivariate normal with mean $\boldsymbol{\mu}_{\beta_i}$ and covariance $\boldsymbol{\Sigma}_{\beta_i}$. Let $\boldsymbol{X}$ be the $2 \times M$ model matrix $(1, \upsilon_i)_{i=1}^M$. The posterior distribution of $\boldsymbol{\mu}_{\beta_i}$ is multivariate normal with mean

$$\left(\sigma_i^{-2} \boldsymbol{X}^{\mathsf{T}} \boldsymbol{R}^{-1} \boldsymbol{X} + \boldsymbol{\Sigma}_{\beta_i}^{-1}\right)^{-1} \left(\boldsymbol{\Sigma}_{\beta_i}^{-1} \boldsymbol{\mu}_{\beta_i} + \sigma_i^{-2} \boldsymbol{X}^{\mathsf{T}} \boldsymbol{R}^{-1} \tilde{\boldsymbol{\theta}}_i\right)$$

and covariance matrix

$$\left(\sigma_i^{-2} \boldsymbol{X}^{\mathsf{T}} \boldsymbol{R}^{-1} \boldsymbol{X} + \boldsymbol{\Sigma}_{\beta_i}^{-1}\right)^{-1}.$$

Acknowledgment

We thank two anonymous reviewers and an anonymous associate editor for their very helpful comments in improving this work. We also thank Dr. Andrew R. Ednie and Dr. Eric S. Bennett for sharing their datasets.

Funding

The authors acknowledge the support from the National Science Foundation (CMMI-1266331, CMMI-1266025).

References

Achard, P., and De Schutter, E. (2006), "Complex Parameter Landscape for a Complex Neuron Model," *PLoS Computational Biology*, 2, e94. [506]

Arendt, P. D., Apley, D. W., and Chen, W. (2012), "Quantification of Model Uncertainty: Calibration, Model Discrepancy, and Identifiability," *Journal of Mechanical Design*, 134, 100908. [500]

Bayarri, M. J., Berger, J. O., Paulo, R., Sacks, J., Cafeo, J. A., Cavendish, J., Lin, C.-H., and Tu, J. (2007), "A Framework for Validation of Computer Models," *Technometrics*, 49, 138–154. [500]

Bear, M. F., Connors, B. W., and Paradiso, M. A. (2007), *Neuroscience* (Vol. 2), Baltimore, MD: Lippincott Williams & Wilkins. [501]

Bondarenko, V. E., Szigeti, G. P., Bett, G. C., Kim, S.-J., and Rasmusson, R. L. (2004), "Computer Model of Action Potential of Mouse Ventricular Myocytes," *American Journal of Physiology-Heart and Circulatory Physiology*, 287, H1378–H1403. [501,507]

Box, G. E., and Hunter, W. G. (1962), "A Useful Method for Model-Building," *Technometrics*, 4, 301–318. [500]

Britton, O. J., Bueno-Orovio, A., Van Ammel, K., Lu, H. R., Towart, R., Gallacher, D. J., and Rodriguez, B. (2013), "Experimentally Calibrated Population of Models Predicts and Explains Intersubject Variability

in Cardiac Cellular Electrophysiology," *Proceedings of the National Academy of Sciences*, 110, E2098–E2105. [506]

Bueno-Orovio, A., Sánchez, C., Pueyo, E., and Rodriguez, B. (2014), "Na/K Pump Regulation of Cardiac Repolarization: Insights From a Systems Biology Approach," *Pflügers Archiv-European Journal of Physiology*, 466, 183–193. [502]

Clancy, C. E., and Rudy, Y. (1999), "Linking a Genetic Defect to Its Cellular Phenotype in a Cardiac Arrhythmia," *Nature*, 400, 566–569. [500,501,502,504,505]

Cotter, S., Roberts, G., Stuart, A., and White, D. (2013), "MCMC Methods for Functions: Modifying Old Algorithms to Make Them Faster," *Statistical Science*, 28, 424–446. [507]

Csilléry, K., Blum, M. G., Gaggiotti, O. E., and François, O. (2010), "Approximate Bayesian Computation (ABC) in Practice," *Trends in Ecology & Evolution*, 25, 410–418. [506]

Currin, C., Mitchell, T., Morris, M., and Ylvisaker, D. (1991), "Bayesian Prediction of Deterministic Functions, With Applications to the Design and Analysis of Computer Experiments," *Journal of the American Statistical Association*, 86, 953–963. [502]

Du, D., Yang, H., Norring, S., and Bennett, E. (2014), "In-Silico Modeling of Glycosylation Modulation Dynamics in HERG Ion Channels and Cardiac Electrical Signals," *IEEE Journal of Biomedical and Health Informatics*, 18, 205–214. [504]

Ednie, A., and Bennett, E. (2012), "Modulation of Voltage-Gated Ion Channels by Sialylation," *Comprehensive Physiology*, 2, 1269–1301. [504]

Ednie, A. R., Horton, K.-K., Wu, J., and Bennett, E. S. (2013), "Expression of the Sialyltransferase, ST3Gal4, Impacts Cardiac Voltage-Gated Sodium Channel Activity, Refractory Period and Ventricular Conduction," *Journal of Molecular and Cellular Cardiology*, 59, 117–127. [500,501,502,504,505]

Gelman, A., Carlin, J. B., Stern, H. S., and Rubin, D. B. (2014), *Bayesian Data Analysis* (Vol. 2), Boca Raton, FL: CRC Press. [502,503]

Grant, A. O. (2009), "Cardiac Ion Channels," *Circulation: Arrhythmia and Electrophysiology*, 2, 185–194. [500]

Grashow, R., Brookings, T., and Marder, E. (2009), "Reliable Neuromodulation From Circuits With Variable Underlying Structure," *Proceedings of the National Academy of Sciences*, 106, 11742–11746. [506]

Handcock, M. S., and Stein, M. L. (1993), "A Bayesian Analysis of Kriging," *Technometrics*, 35, 403–410. [507]

Higdon, D., Gattiker, J., Williams, B., and Rightley, M. (2008), "Computer Model Calibration Using High-Dimensional Output," *Journal of the American Statistical Association*, 103, 570–583. [500]

Hille, B. (2001), *Ion Channels of Excitable Membranes* (Vol. 507), Sunderland, MA: Sinauer. [500]

Hodgkin, A. L., and Huxley, A. F. (1952), "A Quantitative Description of Membrane Current and Its Application to Conduction and Excitation in Nerve," *Journal of Physiology*, 117, 500. [500]

Huxley, A. (2002), "From Overshoot to Voltage Clamp," *Trends in Neurosciences*, 25, 553–558. [501]

Joseph, V. R., and Yan, H. (2015), "Engineering-Driven Statistical Adjustment and Calibration," *Technometrics*, 57, 257–267. [500]

Kass, R. E., Carlin, B. P., Gelman, A., and Neal, R. M. (1998), "Markov Chain Monte Carlo in Practice: A Roundtable Discussion," *The American Statistician*, 52, 93–100. [504]

Kennedy, M. C., and O'Hagan, A. (2001), "Bayesian Calibration of Computer Models," *Journal of the Royal Statistical Society*, Series B, 63, 425–464. [500,502]

Kurtz, T. G. (1971), "Limit Theorems for Sequences of Jump Markov Processes Approximating Ordinary Differential Processes," *Journal of Applied Probability*, 8, 344–356. [501]

Monteiro, J. V., Banerjee, S., and Ramachandran, G. (2014), "Bayesian Modeling for Physical Processes in Industrial Hygiene Using Misaligned Workplace Data," *Technometrics*, 56, 238–247. [500]

Montpetit, M. L., Stocker, P. J., Schwetz, T. A., Harper, J. M., Norring, S. A., Schaffer, L., North, S. J., Jang-Lee, J., Gilmartin, T., Head, S. R., Haslam, S. M., Dell, A., Marth, J. D., and Bennett, E. S. (2009), "Regulated and Aberrant Glycosylation Modulate Cardiac Electrical Signaling," *Proceedings of the National Academy of Sciences*, 106, 16517–16522. [500,504]

Neal, R. M. (2011), "MCMC Using Hamiltonian Dynamics," in *Handbook of Markov Chain Monte Carlo*, eds. S. Brooks, A. Gelman, G. Jones, and X.-L. Meng, Boca Raton, FL: CRC Press, pp. 113–162. [507]

Neher, E., Sakmann, B., and Steinbach, J. H. (1978), "The Extracellular Patch Clamp: A Method for Resolving Currents Through Individual Open Channels in Biological Membranes," *Pflügers Archiv*, 375, 219–228. [501]

Noble, D., Garny, A., and Noble, P. J. (2012), "How the Hodgkin–Huxley Equations Inspired the Cardiac Physiome Project," *Journal of Physiology*, 590, 2613–2628. [501]

Pratola, M. T., Sain, S. R., Bingham, D., Wiltberger, M., and Rigler, E. J. (2013), "Fast Sequential Computer Model Calibration of Large Nonstationary Spatial-Temporal Processes," *Technometrics*, 55, 232–242. [500]

Ramsay, J. O., Hooker, G., Campbell, D., and Cao, J. (2007), "Parameter Estimation for Differential Equations: A Generalized Smoothing Approach," *Journal of the Royal Statistical Society*, Series B, 69, 741–796. [500]

Sacks, J., Welch, W. J., Mitchell, T. J., and Wynn, H. P. (1989), "Design and Analysis of Computer Experiments," *Statistical Science*, 4, 409–423. [502]

Sarkar, A. X., Christini, D. J., and Sobie, E. A. (2012), "Exploiting Mathematical Models to Illuminate Electrophysiological Variability Between Individuals," *Journal of Physiology*, 590, 2555–2567. [506]

Stocker, P. J., and Bennett, E. S. (2006), "Differential Sialylation Modulates Voltage-Gated Na+ Channel Gating Throughout the Developing Myocardium," *Journal of General Physiology*, 127, 253–265. [500]